Energy & Environmental Science

RSC Publishing

COMMUNICATION

View Article Online
View Journal | View Issue

Cite this: *Energy Environ. Sci.*, 2013, **6**, 1791

Received 12th December 2012
Accepted 10th April 2013

DOI: 10.1039/c3ee24345a

www.rsc.org/ees

Shape-tailored TiO_2 nanocrystals with synergic peculiarities as building blocks for highly efficient multi-stack dye solar cells†

Luisa De Marco,[a] Michele Manca,*[a] Roberto Giannuzzi,[a] Maria R. Belviso,[b] P. Davide Cozzoli[bc] and Giuseppe Gigli[abc]

An engineered photoelectrode for dye solar cells has been developed through the combination of three mesoporous stacks made of shape-tailored TiO_2 anatase nanocrystals, which have been *ad hoc* synthesized by suitable colloidal routes. Optimization of light harvesting and charge collection efficiency allowed us to obtain a high power conversion efficiency of 10.26%.

Broader context

The ability to fabricate photoanodes in which structural and morphological features of the TiO_2 building blocks provide tailored nanotextures with a high degree of functionalities still represents a crucial issue towards boosting the ultimate light-to-electricity conversion efficiency of a dye solar cell. With this aim we have recently developed a novel and facile method for preparing high-quality mesoporous multi-layered films which comprise three different breeds of shape-tailored anatase TiO_2 nanorods synthesized by means of suitable non-hydrolytic synthetic routes. This novel multi-stack photoanode enables us to maximize both the key features which generally compete with each other: the light harvesting capability and the charge collection efficiency. A power conversion efficiency as high as 10.26% has been achieved showing a considerable increase with respect to reference conventional materials.

Dye-sensitized solar cells (DSCs) are one of the most promising photovoltaic technologies for production of renewable, clean, and affordable energy.[1] Among third-generation photovoltaic devices DSCs exhibit the highest performance; to date, a record power conversion efficiency (PCE) of 12.3% has been achieved with photoanodes consisting of 20 nm anatase TiO_2 nanocrystallites co-sensitized by YD2-*o*-C8 and Y123 dyes.[2]

As the crystal structure and geometry of the photoelectrode of a DSC are crucial to determining the photoelectrochemical properties of the system, various strategies have been pursued to conveniently engineer photoanodes with tailored features.[3–8] Although a porous electrode made of nanocrystallites with a high internal surface area is essential to guarantee loading of large amounts of dye molecules, the diffusion of electrons is restricted by trapping and detrapping events along defects, surface states, and grain boundaries.[9] A possible solution to improve the charge collection efficiency is the use of anisotropically shaped TiO_2 nanostructures, such as all-linear[10–14] or branched nanorods,[15–17] nanowires[18,19] and nanotubes arrays,[20,21] which are able to provide extended directional pathways for rapid collection of photogenerated electrons. However, modest PCE values have been reported to date, mainly because of the reduced internal surface area offered by photoanodes which employ nanorods or nanowires with a mean size larger than 100 nm[12,22,23] and/or the severe degradation of the original structural–morphological features of the selected anisotropic TiO_2 nanocrystals upon sintering.[11,15,16]

Another versatile strategy to enhance the PCE is the implementation of relatively large nanoparticles (mean size > 400 nm) as scattering centers, which present a well-defined hierarchical nanostructure to ensure an acceptable value of effective surface area.[24,25] However, photoanodes based on these nanomaterials hardly offer any further benefits, such as, for instance efficient charge transport, because electron percolation within nanocrystallites is reasonably expected to be more difficult. Hence, there is still plenty of scope for the design and synthesis of materials which should simultaneously exhibit large surface areas for dye adsorption, efficient light scattering and fast electron transport.

Herein we present an affordable and versatile approach to photoelectrode structuring by which the performance of a DSC can be maximised. Our strategy exploits a new class of hierarchically structured photoanodes consisting of different stacks of purposely selected anisotropically shaped TiO_2 nanocrystals which have been synthesized by advanced wet-chemical routes.

[a]*CBN, Center for Biomolecular Nanotechnologies, Fondazione Istituto Italiano di Tecnologia, Via Barsanti, 73010 Arnesano (Lecce), Italy. E-mail: michele.manca@iit.it*
[b]*National Nanotechnology Laboratory (NNL), CNR Istituto Nanoscienze, c/o Distretto Tecnologico, Via Arnesano km 5, 73100 Lecce, Italy*
[c]*Dipartimento di Matematica e Fisica "E. De Giorgi", Università del Salento, Via per Arnesano, 73100 Lecce, Italy*

† Electronic supplementary information (ESI) available. See DOI: 10.1039/c3ee24345a

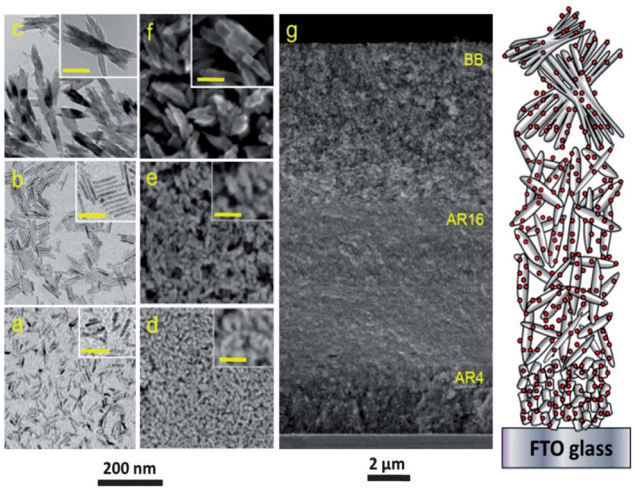

Fig. 1 TEM images of the different anisotropically shaped TiO_2 nanocrystals: (a) AR4-NRs, (b) AR16-NRs and (c) BB-NRs. SEM images of the sintered films made of (d) AR4-NRs, (e) AR16-NRs and (f) BB-NRs. (g) Cross-sectional view of the engineered three-stack photoelectrode along with corresponding sketches highlighting its nano-/micro-structure. Scale bars in the insets represent 50 nm.

Our DSCs comprise three TiO_2 nanocrystal layers with complementary and synergistic properties (see a representative sketch in Fig. 1): a bottom layer made of small nanorods which provide tremendous specific surface area and exceptional transparency across the dye's absorption spectrum; an intermediate layer made of high aspect-ratio nanorods which guarantee superior electron transport and good dye loading capability; a third upper layer made of relatively larger nanorods with hyperbranched topologies, which offer adequate light-scattering capability and enable favourable interfacial charge-transfer.

This fabrication approach leads to DSC photoanodes capable of exhibiting indispensable, yet often incompatible properties that are difficult to accommodate at once, such as high specific surface area, fast electron transport and pronounced light-scattering. The 10.26% efficiency achieved with our multi-layered photoanodes greatly exceeds the record literature values documented so far for TiO_2-nanorod-based DSCs.[14]

Colloidal TiO_2 nanocrystals with one-dimensional linear or branched profiles were prepared by recently developed surfactant-assisted sol–gel routes.[17,26,27] Our syntheses are based on the reaction of a titanium alkoxide in a coordinating mixture of a solvent and suitable alkyl carboxylic acid and/or amines, which regulate the solution supersaturation by forming reactive complexes with the precursor, and drive anisotropic evolution and/or lattice splitting by dynamically adsorbing/desorbing to/from the surface of the growing nanocrystals. Selected protocols have been exploited (detailed procedures are reported in the ESI†) to synthesize three different families of size- and shape-tailored TiO_2 nanocrystals as the starting building blocks for our DSCs. In particular:

- [001]-elongated anatase nanorods (NRs) with short-/long-axis sizes of 3–4 × 12–14 nm (aspect ratio = 4, henceforth referred to as AR4, Fig. 1a) were obtained by trimethylamine *N*-oxide catalyzed hydrolysis of titanium isopropoxide (TTIP) in nonanoic acid.[26]

- [001]-elongated linear anatase NRs with sizes of 3–4 × 45–50 nm (aspect ratio = 16, AR16, Fig. 1b) were synthesized by non-hydrolytic condensation of TTIP in oleic acid.[27]

- Hyperbranched anatase NRs with overall projected sizes of 30–50 × 180–200 nm, characterized by variable braid- to sheaf-like profiles arising from the bandaging of numerous (>10) [001]-oriented 3–5 × 80–100 nm filaments at their median point (referred to as BB, Fig. 1c) were synthesized by aminolytic decomposition of titanium oleate complexes at high temperatures.[17]

In all cases the as-prepared NRs were surface-capped with a hydrophobic oleate surfactant shell that guaranteed kinetic stabilization against undesired irreversible coalescence phenomena and ensured retention of the size/shape features during post-synthesis processing, including the thermal sintering step required for photoanode assembly.[13,17,28]

SEM images (Fig. 1d–f and S1†) clearly revealed the unique morphologies of the as-prepared films: TiO_2 nanocrystals with anisotropically tailored linear and branched shapes were safely processed with intact geometric features (*cf.* images in Fig. 1a–f) into high-quality mesoporous photoelectrodes without collapsing into macroscopic segregated agglomerates and/or generating extensive cracks. The XRD patterns of these films (see Fig. S2 in ESI†) confirmed retention of the anatase crystal structure of the original nanocrystals, without any detectable secondary phases.

As the photovoltaic performances of DSCs are strictly related to the morphology of the photoanode's building blocks, we investigated the structure–performance relationship in DCSs individually made from a single breed of nanocrystals.[28] Efficiencies of the three species of NR-based PEs are listed in Table 1, whereas the *J*–*V* curves are shown in Fig. 2. The following observations could be outlined.

Table 1 Photovoltaic parameters of DSCs based on the synthesized NRs and Dyesol colloidal pastes measured upon application of a 0.25 cm^2 black mask under 1 sun illumination (AM 1.5, 100 mW cm^{-2})

Device	η%	FF	V_{OC} (V)	J_{SC} (mA cm^{-2})	Dye loading (mol cm^{-2}) × 10^{-7}
AR4: 3 μm	4.46	0.71	0.79	7.95	0.72
AR16: 3 μm	4.15	0.71	0.82	7.12	0.57
BB: 3 μm	3.53	0.73	0.84	5.75	0.31
AR4: 7 μm	5.95	0.70	0.79	10.76	1.67
AR16: 7 μm	7.20	0.70	0.81	12.70	1.21
BB: 7 μm	5.44	0.72	0.82	9.22	0.74
AR4 + AR16: 3 + 4 = 7 μm	7.49	0.69	0.81	13.41	1.38
ML-DSC 17 μm (3 AR4 + 7 AR16 + 7 BB)[a]	10.26	0.70	0.81	18.10	2.68
D-DSC 17 μm (12 18NR-T + 5 18NR-AO)[a]	8.21	0.69	0.79	15.06	1.97

[a] Note that the values reported in this table represent one single device; further details about reproducibility and the dispersion in the values are reported in the ESI (Table S2).

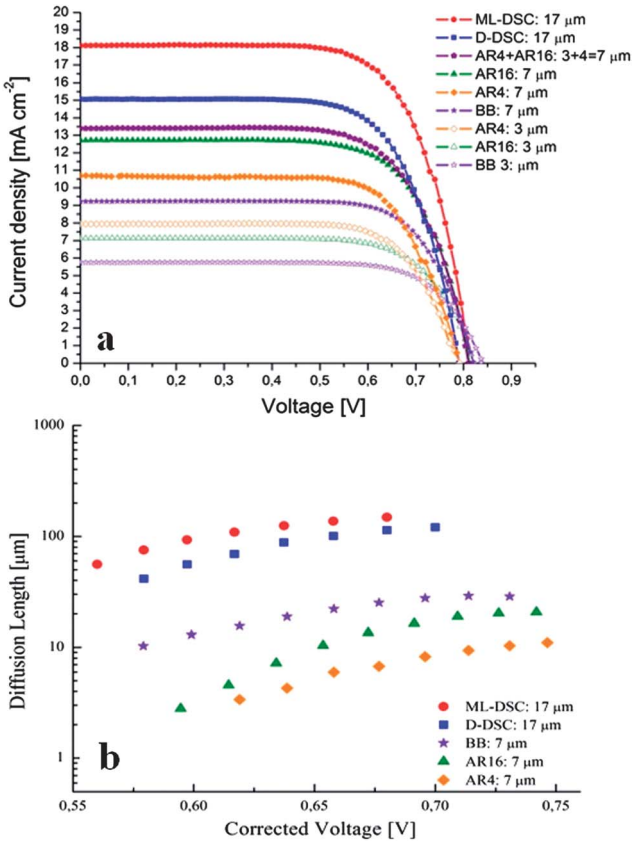

Fig. 2 (a) *J–V* curves of DSCs based on NRs and on standard materials and (b) electron diffusion length of different PEs.

- At relatively low thicknesses (3 μm), AR4-based photoelectrodes (PEs) showed the best performances, in good agreement with their superior dye-loading capability.

- As the thickness grew up to 7 μm, the performance of PEs constituted by AR16 nanorods overcame that of the corresponding AR4-based mesoporous films, despite their relatively lower surface area. The increased short current density (J_{SC}) correlated with the superior charge transport properties of NRs with a higher aspect-ratio. As shown in Fig. 2b, AR16-PEs were indeed characterized by an electron diffusion length[29] which was almost twice that found for their homologous shorter NRs. These pieces of evidence corroborated the conclusion that the inherent electron transport properties of the films did have a tremendous impact on their ultimate photovoltaic performances.

These observations suggested us to exploit the possible synergistic effects of a suitable combination of AR4- and AR16-based films in the frame of a bi-layer architecture. Such a structure actually demonstrated to be even more efficient than the corresponding monolayers: a 7 μm thick PE composed of an AR4-based bottom layer (thickness 3 μm) and an AR16-based top layer (thickness 4 μm) indeed generated a short-circuit current density as high as 13.41 mA cm^{-2}, when compared with the values of 10.76 and 12.70 mA cm^{-2} which were measured in the case of 7 μm thick AR4- and AR16-PEs, respectively.

AR4 and AR16 films resulted in being highly transparent prior to being dye-sensitized (see Fig. S3†) due to the homogeneous assembly of the small sized nanocrystals, which prevented light-scattering effects from being originated in these films. This fact implied that further enhancement of the photovoltaic performances of our NR-based PEs should be achievable through the introduction of a suitable photon-recycling structure. PEs based on nanorod bundles, BB-NRs, with relatively larger dimensions were verified to work as light-scattering centres while maintaining good dye loading capability and allowing a surprisingly high photocurrent density (9.22 mA cm^{-2} for 7 μm thick PEs). These photoanodes were indeed characterized by the longest value of the electron diffusion length (see Fig. 2b), which is almost two times higher than AR16-PE and three times higher than AR4-PEs. They also offered the most favourable conditions under which recombination at the interface with the electrolyte could be minimized, as demonstrated by their high open-circuit voltage (0.82 V). This result could be ascribed to the particular bundle-like architecture concerned with their monocrystalline nature, where the individual rod-shaped arms were assembled so as to guarantee crystal lattice continuity at the relevant branch points and, hence, to dramatically reduce the density of electron trap states at surfaces and grain boundaries.[17]

We thus made use of all findings to design and fabricate an engineered PE which embodied all of the three families of the synthesized shape-tailored TiO_2 nanocrystals within a unique multistack architecture in such a way as to complementarily and synergistically exploit the properties associated with their respective topological features. The deposition of a BB-based layer on the top of the AR4 + AR16 PE was revealed to be the most suitable approach to generate effective light scattering without detrimentally sacrificing any other desirable properties, as well as the surface area and electron transport. The thickness of each layer was tuned in a range comprised between 3 and 7 μm with the aim of optimizing the balance among the specific characteristics of the three nanostructures. The performances obtained with DSCs based on different photoanode configurations are reported in the ESI section (Table S1).†

A PCE as high as 10.26% was achieved with a 17 μm thick photoanode (ML-DSC) which incorporated a bottom layer (3 μm) made of AR4-NRSs, a middle layer (7 μm) made of AR16-NRs and a top layer (7 μm) made of hyperbranched BB. A cross-sectional SEM image of such a nanostructured film is reported in Fig. 1g. The resulting photovoltaic parameters are summarized in Table 1 and *J–V* curves are shown in Fig. 2. ML-DSCs were distinguished by a J_{SC} of 18.10 mA cm^{-2}, an open-circuit voltage (V_{OC}) of 0.81 V and a fill factor (FF) of 0.70, while a standard double-layer nanoparticles-based photoanode (D-DSC) with the same thickness gave a PCE of only 8.21% and a J_{SC} of 15.06 mA cm^{-2}.

The increased efficiency of our ML-DSC was primarily due to the enhancement in J_{SC} that could be related to the overall larger dye amount adsorbed onto a ML film (2.68×10^{-7} mol cm^{-2}), being higher than that of the reference D-DSC film (1.97×10^{-7} mol cm^{-2}). These properties could be ascribed to the larger specific surface area of the ML film, mainly derived

from the introduction of the AR4 and AR16 layers. In addition, another factor contributing to enhance the performance of the ML-DSC should be the significant improvement of the charge-collection efficiency, as demonstrated by the trend of the electron diffusion length reported in Fig. 2b. The diffusion length of our ML-PEs indeed resulted in being 30% longer with respect to the case of D-DSCs.

A further elucidative insight into their electrochemical behaviour of the ML-DSC was provided by the estimation of the apparent electron lifetime, τ_n.[30] It was verified that in our engineered multi-stack PEs, the photogenerated electrons were characterized by a considerably longer apparent electron lifetime under the open-circuit condition (τ_n = 154 ms) with respect to the nanoparticles-based PE used as a reference (τ_n = 111 ms). This fact further confirmed their superior property of preventing the electrons from recombining with existing oxidized species, such as I_3^- in the electrolyte. As a consequence, the modest increment of V_{OC} observed in the ML-DSC (0.81 V *vs.* 0.79 V) should be intrinsically correlated with the observed reduction of the dark current (see Fig. S4†).

Besides this, an important contribution to the boosting of J_{SC} was related to the enhancement of the light scattering effect in ML PEs with respect to AR4 + AR16 PEs. The reflectance spectrum of a 7 μm thick BB layer is shown in Fig. 3a along with those of a commercial scattering layer (Dyesol 18NR-AO, thickness 5 μm) and of a 10 μm thick AR4 + AR16 bi-layer structure. As expected, both the commercial and our BB-based films exhibited dramatically higher diffuse reflection in the visible range with respect to the AR4 + AR16 PE.

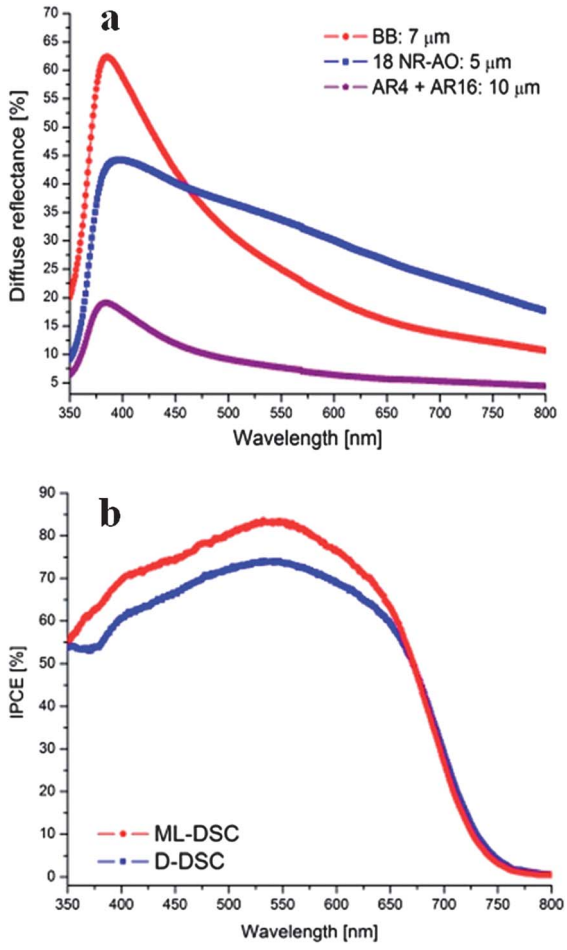

Fig. 3 (a) Diffuse-reflectance spectra of the BB-NR film, AR4 + AR16 film and 18NR-AO film; (b) IPCE spectra of D-DSCs and ML-DSCs.

The IPCE spectrum of the ML-DSC (see Fig. 3b) resulted in being shifted upwards with respect to the reference cell (the topmost value passed from 75% up to 83%). This improvement, which was maintained over a wide range (350–600 nm), could, however, be only partially ascribed to the scattering effect of the upper BB-layer; rather it should be attributed to the extended dye loading capability and to the improved electron transport through the TiO_2 nanorod network. The photon recycling effect of the BB-layer was proven to be beneficial only within a limited range of wavelengths since, as is well known, it strongly depends on the size of nanoparticles.[31] The reflectivity of the BB-layer was in fact higher than those observed for the Dyesol 18NR-AO (which embodied 300 nm sized diffusing nanoparticles) only in the range between 350 and 470 nm. At higher wavelengths – corresponding to the region of maximum absorption of N719 – the scattering effect of the BB attenuated and the gap in the IPCE spectra tended to vanish. This observation suggests that further optimization of the three-layer architecture proposed by us should be achievable through the implementation of an additional scattering layer made of much larger nanocrystals.

To summarize, we have proposed a novel engineered multistack electrode which comprises three different breeds of shape-tailored TiO_2 NRs and enables control over the electron transport and the recombination dynamics as well as over the optical scattering. Suitable adjustment of the shape and size of the NRs made it possible to simultaneously maximize the key features of a photoelectrode, which are generally incompatible with each other: the light harvesting capability and the charge collection efficiency. A power conversion efficiency as high as 10.26% was reported for a dye solar cell made of a 17 μm-thick three-stack photoelectrode and a consistent improvement was assessed with respect to a reference photoelectrode made from conventional spherical nanoparticles. Our work demonstrates that the ability to create photoanodes in which the structural and morphological features of the primitive nanocrystalline building blocks can provide tailored nanotextures with a higher degree of functionality represents an indispensable step towards boosting the ultimate light-to-electricity conversion of a DSC.

This work was supported by the European project ESCORT—Efficient Solar Cells based on Organic and Hybrid Technology (7^{th} FWP—reference number 261920) and by the national projects EFOR (L. 191/2009 art. 2 comma 44), DSSCX (MIUR-PRIN 2010–2011 – 20104XET32), AEROCOMP (contract MIUR no. DM48391), MAAT (MIUR – PON02_00563_3316357 – CUP B31C12001230005). The authors thank Paola Pareo and Rita Agosta for the precious technical support and Filippo De Angelis for helpful discussions. Daunia Wind is gratefully acknowledged for funding.

Notes and references

1 A. Hagfeldt, G. Boschloo, L. Sun, L. Kloo and H. Pettersson, *Chem. Rev.*, 2010, **110**, 6595.
2 A. Yella, H. W. Lee, H. N. Tsao, C. Yi, A. K. Chandiran, M. K. Nazeeruddin, E. W. G. Diau, C. Y. Yeh, S. M. Zakeeruddin and M. Grätzel, *Science*, 2011, **334**, 629.
3 J. Du, J. Qi, D. Wang and Z. Tang, *Energy Environ. Sci.*, 2012, **5**, 6914.
4 R. Agosta, R. Giannuzzi, L. De Marco, M. Manca, M. R. Belviso, P. D. Cozzoli and G. Gigli, *J. Phys. Chem. C*, 2013, **117**(6), 2574.
5 L. Han, A. Islam, H. Chen, C. Malapaka, B. Chiranjeevi, S. Zhang, X. Yang and M. Yanagida, *Energy Environ. Sci.*, 2012, **5**, 6057.
6 N. Tétreault and M. Grätzel, *Energy Environ. Sci.*, 2012, **5**, 8506.
7 Z. Dong, X. Lai, J. E. Halpert, N. Yang, L. Yi, J. Zhai, D. Wang, Z. Tang and L. Jiang, *Adv. Mater.*, 2012, **24**, 1046.
8 J.-H. Yum, E. Baranoff, S. Wenger, M. K. Nazeeruddin and M. Grätzel, *Energy Environ. Sci.*, 2011, **4**, 842.
9 N. Kopidakis, K. D. Benkstein, J. van de Lagemaat and A. J. Frank, *J. Phys. Chem. B*, 2003, **107**, 11307.
10 J. Jiu, S. Isoda, F. Wang and M. Adachi, *J. Phys. Chem. B*, 2006, **110**, 2087.
11 S. H. Kang, S. H. Choi, M. S. Kang, J. Y. Kim, H. S. Kim, T. Hyeon and Y. E. Sung, *Adv. Mater.*, 2008, **20**, 54.
12 S. Lee, I. S. Cho, J. H. Lee, D. H. Kim, D. W. Kim, J. Y. Kim, H. Shin, J. K. Lee, H. S. Jung, N. G. Park, K. Kim, M. J. Ko and K. S. Hong, *Chem. Mater.*, 2010, **22**, 1958.
13 L. De Marco, M. Manca, R. Giannuzzi, F. Malara, G. Melcarne, G. Ciccarella, I. Zama, R. Cingolani and G. Gigli, *J. Phys. Chem. C*, 2010, **114**, 4228.
14 Y. Qiu, W. Chen and S. Yang, *Angew. Chem., Int. Ed.*, 2010, **49**, 3675.
15 J. K. Oh, J. K. Lee, H. S. Kim, S. B. Han and K. W. Park, *Chem. Mater.*, 2010, **22**, 1114.
16 B. Koo, J. Park, Y. Kim, S. H. Choi, Y. E. Sung and T. Hyeon, *J. Phys. Chem. B*, 2006, **110**, 24318.
17 R. Buonsanti, E. Carlino, C. Giannini, D. Altamura, L. De Marco, R. Giannuzzi, M. Manca, G. Gigli and P. D. Cozzoli, *J. Am. Chem. Soc.*, 2011, **133**, 19216.
18 X. Feng, K. Zhu, A. J. Frank, C. A. Grimes and T. E. Mallouk, *Angew. Chem., Int. Ed.*, 2012, **51**, 2727.
19 X. Feng, K. Shankar, O. K. Varghese, M. Paulose, T. J. Latempa and C. A. Grimes, *Nano Lett.*, 2008, **8**, 3781.
20 Q. Zheng, H. Kang, J. Yun, J. Lee, J. H. Park and S. Baik, *ACS Nano*, 2011, **5**, 5088.
21 M. Ye, X. Xin, C. Lin and Z. Lin, *Nano Lett.*, 2011, **11**, 3214.
22 I. C. Baek, M. Vithal, J. A. Chang, J. H. Yum, M. K. Nazeeruddin, M. Grätzel, Y. C. Chung and S. I. Seok, *Electrochem. Commun.*, 2009, **11**, 909.
23 E. Ghadiri, N. Taghavinia, S. M. Zakeeruddin, M. Grätzel and J. E. Moser, *Nano Lett.*, 2010, **10**, 1632.
24 F. Huang, D. Chen, X. L. Zhang, R. A. Caruso and Y. B. Cheng, *Adv. Funct. Mater.*, 2010, **20**, 1301.
25 Y. C. Park, Y. J. Chang, B. G. Kum, E. H. Kong, J. Y. Son, Y. S. Kwon, T. Park and H. M. Jang, *J. Mater. Chem.*, 2011, **21**, 9582.
26 L. De Caro, E. Carlino, G. Caputo, P. D. Cozzoli and C. Giannini, *Nat. Nanotechnol.*, 2010, **5**, 360.
27 J. Joo, S. G. Kwon, T. Yu, M. Cho, J. Lee, J. Yoon and T. Hyeon, *J. Phys. Chem. B*, 2005, **109**, 15297.
28 L. De Marco, M. Manca, R. Buonsanti, R. Giannuzzi, F. Malara, P. Pareo, L. Martiradonna, N. M. Giancaspro, P. D. Cozzoli and G. Gigli, *J. Mater. Chem.*, 2011, **21**, 13371.
29 J. Bisquert, *Phys. Chem. B*, 2002, **106**, 325.
30 J. Bisquert, F. Fabregat-Santiago, I. Mora-Serò, G. Garcia-Belmonte and S. Gimènez, *J. Phys. Chem. C*, 2009, **113**, 17278.
31 W. E. Vargas, *J. Appl. Phys.*, 2000, **88**, 4079.